Journal of Cerebral Blood Flow & Metabolism (2011) 31, 1051–1063

www.jcbfm.com

Microvascular oxygen tension and flow measurements in rodent cerebral cortex during baseline conditions and functional activation

Mohammad A Yaseen[1], Vivek J Srinivasan[1], Sava Sakadžić[1], Harsha Radhakrishnan[1], Iwona Gorczynska[2], Weicheng Wu[1], James G Fujimoto[2] and David A Boas[1]

[1]*Department of Radiology, MGH/MIT/HMS Athinuola A. Martinos Center for Biomedical Imaging, Massachusetts General Hospital, Harvard Medical School, Charlestown, Massachusetts, USA;* [2]*Department of Electrical Engineering and Computer Science and Research Laboratory of Electronics, Massachusetts Institute of Technology, Cambridge, Massachusetts, USA*

Measuring cerebral oxygen delivery and metabolism microscopically is important for interpreting macroscopic functional magnetic resonance imaging (fMRI) data and identifying pathological changes associated with stroke, Alzheimer's disease, and brain injury. Here, we present simultaneous, microscopic measurements of cerebral blood flow (CBF) and oxygen partial pressure (pO_2) in cortical microvessels of anesthetized rats under baseline conditions and during somatosensory stimulation. Using a custom-built imaging system, we measured CBF with Fourier-domain optical coherence tomography (OCT), and vascular pO_2 with confocal phosphorescence lifetime microscopy. Cerebral blood flow and pO_2 measurements displayed heterogeneity over distances irresolvable with fMRI and positron emission tomography. Baseline measurements indicate O_2 extraction from pial arterioles and homogeneity of ascending venule pO_2 despite large variation in microvessel flows. Oxygen extraction is linearly related to flow in ascending venules, suggesting that flow in ascending venules closely matches oxygen demand of the drained territory. Oxygen partial pressure and relative CBF transients during somatosensory stimulation further indicate arteriolar O_2 extraction and suggest that arterioles contribute to the fMRI blood oxygen level dependent response. Understanding O_2 supply on a microscopic level will yield better insight into brain function and the underlying mechanisms of various neuropathologies.
Journal of Cerebral Blood Flow & Metabolism (2011) **31,** 1051–1063; doi:10.1038/jcbfm.2010.227; published online 22 December 2010

Keywords: cerebral blood flow; fMRI; microscopy; optical imaging; oxygen

Introduction

Brain tissue relies heavily upon a constant and dependable supply of metabolites such as oxygen and glucose. Under normal resting conditions, neural activity and cerebral blood flow (CBF) are tightly coupled, providing steady and sufficient amounts of these metabolites while removing carbon dioxide, heat, and other by-products (Sokoloff, 1992).

Correspondence: Associate Professor DA Boas, Massachusetts General Hospital, Department of Radiology, Martinos Center for Biomedical Imaging, Harvard Medical School, Charlestown, MA 02129, USA.
E-mail: dboas@nmr.mgh.harvard.edu;
Web: http://www.nmr.mgh.harvard.edu/PMI/index.html
This study was supported by NIH R01-NS057476, P50-NS010828, K99NS067050, P01-NS055104, and Air Force Office of Scientific Research FA9550-07-1-0101.
Received 16 September 2010; revised 17 November 2010; accepted 26 November 2010; published online 22 December 2010

Although it has long been presumed that oxidative metabolism is the primary mechanism to satisfy the brain's energetic demands, the influence and dynamics of oxygen supply remain ambiguous (Bartlett *et al*, 2008; Riera *et al*, 2008). During both resting and activated conditions, the blood's supply of oxygen exceeds the brain's energetic demand. Numerous studies have demonstrated that the brain's hemodynamic response to evoked functional stimulation, which consists of increases in CBF, cerebral blood volume (CBV), and cerebral metabolic rate of oxygen ($CMRO_2$), involves the dynamic uncoupling of CBF and oxygen consumption, with disproportionately larger increases in CBF compared with $CMRO_2$. Using techniques such as functional magnetic resonance imaging (fMRI), positron emission tomography (PET), and near infrared spectroscopy (NIRS), these investigations have demonstrated that evoked functional stimulation yields increases in CBF between 1.5 and 6 times larger than $CMRO_2$ increases (Boas *et al*, 2003; Leontiev *et al*, 2007; Vafaee and Gjedde, 2004).

The role of the hemodynamic response, in particular, the role of increased vascular oxygen supply during evoked stimulation remains a subject of tremendous interest. The decrease in oxygen extraction fraction resultant from increased CBF yields a transient decrease in deoxyhemoglobin during functional activation. This change in paramagnetic deoxyhemoglobin content serves as the mechanism by which the blood oxygen level dependent (BOLD) signal in fMRI identifies local changes in cerebral activity (Kwong *et al*, 1992). Measuring the BOLD response has lead to wide use of fMRI to noninvasively map regions of evoked cerebral activation in the human brain. However, accurate, quantitative interpretation of the cellular activity giving rise to these BOLD observations remains ambiguous (Atwell and Iadecola, 2002; Sokoloff, 2008). The measured change in deoxyhemoglobin depends highly upon baseline conditions of oxygen supply and is ultimately limited by the amount of deoxyhemoglobin present in the capillaries and veins. The magnitude of the BOLD response therefore does not provide a quantitative measure of neuronal function. Additionally, the spatial extent of the hemodynamic response may be larger or displaced from the site of activated brain tissue. It has been suggested that the BOLD response is sensitive primarily to pronounced changes in deoxyhemoglobin content observed in downstream venules, potentially distant from the actual region of neural activity (Buxton, 2010). Recent experiments have suggested that significant deoxyhemoglobin changes also occur in the arterioles and may confound interpretation of the BOLD signal (Hillman *et al*, 2007; Vazquez *et al*, 2010). Detailed microscopic measurements of the variation in blood flow and oxygen content in cerebral microvasculature are needed to better guide interpretation of macroscopic measures such as fMRI BOLD.

We have developed an optical imaging system for measuring cerebral oxygenation and hemodynamics in rodent brains with high spatial and temporal resolution. The multimodal system uses Fourier-domain Doppler optical coherence tomography (OCT) (Leitgeb *et al*, 2003) to measure CBF and confocal microscopy to measure cerebral pO_2 using the phosphorescence-quenching method (Rumsey *et al*, 1988). Compared with traditional imaging techniques such as fMRI and positron emission tomography, the multimodal optical system offers advantages by performing direct, nondestructive measurements of absolute cerebral oxygenation and blood flow simultaneously within individual microvessels with high temporal resolution. Unlike fMRI and positron emission tomography, however, light absorption and scattering effects of brain tissue limits the system to measuring these parameters in superficial cortical vessels of the exposed brain.

Here, we present OCT CBF and confocal pO_2 data acquired simultaneously in the cortical microvessels of anesthetized rats under baseline conditions and during functional somatosensory stimulation. Baseline results suggest that O_2 extraction occurs in diving pial arterioles and reveal a linear relationship between absolute CBF and oxygen extraction. Oxygen partial pressure and relative CBF (rCBF) transients during somatosensory stimulation further indicate arteriolar O_2 extraction. Temporal delays were observed between venous CBF and pO_2 transients during stimulation.

Our observations of simultaneous CBF and pO_2 on a microscopic scale will yield greater insight in interpreting the macroscopic BOLD response. In particular, our results imply that arterioles may contribute to the early onset of the observed BOLD response. Additionally, a more detailed understanding of cerebral vascular oxygen supply could lead to better diagnosis and treatment of pathological disorders whose symptoms include disruption of coupling between oxygen supply and demand, including stroke and Alzheimer's disease.

Materials and methods

Multimodal Imaging System

Figure 1 depicts our multimodal OCT and confocal imaging system (Srinivasan *et al*, 2009; Yaseen *et al*, 2009). A superluminescent diode (Exalos, Inc., Langhorn, PA, USA) operating at $\sim$856 nm with 54 nm bandwidth operated as the light source for OCT. Power on the sample was 1.5 mW, with 99 dB sensitivity. Galvanometer scanner mirrors (Cambridge Technology, Inc., Lexington, MA, USA) were relay imaged to the back focal plane of the microscope objective (Olympus XLFluor $\times$4, 0.28 NA, Center Valley, PA, USA). Back reflected light from the sample was recombined with light reflected from a reference arm. The recombined light was spectrally resolved using a diffraction grating and collected with a 2048 pixel, 12-bit line scan camera (Aviiva SM2 camera, e2v semiconductors, Chelmsford, Essex, UK). The camera and custom software enabled an imaging speed of 22,000 axial scans per second and an axial imaging range of 2.5 mm in air. Maximal depth resolution was $\sim$6.4 μm in air (4.8 μm in tissue).

Excitation light for the confocal portion of the system was provided by a CW diode laser (λ = 532 nm; B&W Tek, Inc., Newark, Delaware, USA) temporally gated by an electrooptical modulator (ConOptics, Inc., Danbury, CT, USA) with an extinction ratio of $\sim$200. The excitation beam passed through a beam expanding telescope, polarizer, shutter, dichroic mirror, scan lens, and tube lens. A second set of galvanometer scanners guided the confocal excitation beam to selected intravascular locations on the cortical surface. Average excitation power on the sample was $\sim$10 to 15 mW. Absolute measurements of pO_2 in various cortical microvessels were performed by administering Oxyphor R2, the O_2-sensitive porphyrin-based phosphor dye (Oxygen Enterprises, Philadelphia, PA, USA) (Vinogradov *et al*, 1999). The emitted phosphorescence light was descanned and collected using an avalanche photodiode photon counting module (SPCM-AQRH-10, Perkin-Elmer, Inc., Waltham, MA, USA) with 50 MHz sampling rate. The avalanche photodiode

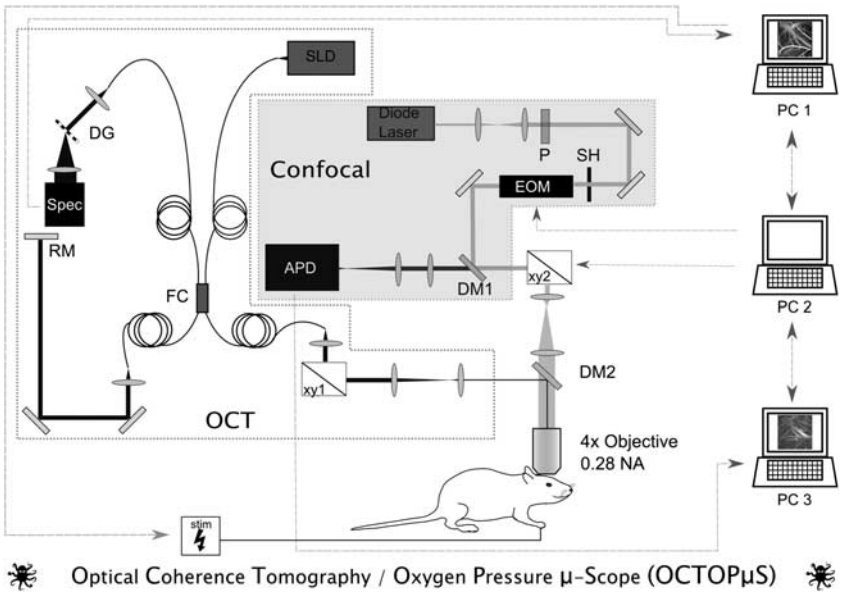

Figure 1 Custom-designed multimodal imaging system. Using a superluminescent diode (SLD) light source, a pair of galvanometric scanner mirrors (xy1), diffraction grating (DG), and spectrometer the optical coherence tomography (OCT) component of the system measures cerebral blood flow (CBF) in individual microvessels. Concurrently, the confocal component uses a 532-nm diode laser excitation source, polarizer (P), electrooptical modulator (EOM), galvanometric scanners (*xy*2), pinhole spatial filter (P), and avalanche photodiode detector (APD) to measure vascular oxygen partial pressure (pO_2). Both system components deliver and detect signal to and from the exposed rat cortex through a $\times 4$ 0.28 NA objective lens. With custom-built software, PC1 controls the OCT acquisition and functional stimulator (stim), whereas PC2 and PC3 control and record signals from the confocal system, respectively.

detector's active area (180 μm diameter) functioned as a pinhole for confocal detection.

Custom-written software and a custom-designed dichroic mirror (DM2 $\lambda_{cutoff} = 750$ nm; Chroma Technologies, Bellows Falls, VT, USA) enabled simultaneous acquisition of CBF and pO_2 with high spatial and temporal resolution.

Animal Preparation

Animals were prepared in accordance with a protocol approved by the Subcommittee on Research Animal Care at the Massachusetts General Hospital. A sealed cranial window was created over the somatosensory cortices of male Sprague-Dawley rats (250 to 400 g). Tracheotomy and cannulation of the femoral artery and vein were performed under isoflurane anesthesia ($\sim$2%). The scalp was retracted after fixing the head in a stereotactic frame. Using a saline-cooled dental drill, sections of the skull and dura mater were removed, exposing the somatosensory cortex ($\sim 3 \times 3$ mm^2). Following exposure, the brain surface was covered with agarose gel and a glass cover slip and sealed with dental acrylic cement. After the craniotomy, isoflurane was discontinued and replaced with a continuous infusion of α-chloralose (30 mg/kg per hour). Arterial blood pressure, heart rate, body temperature, and blood gas measurements were monitored continuously throughout the experiments. Body temperature and breathing were controlled with a thermocouple-monitored heating blanket (Harvard Apparatus, Holliston, MA, USA) and a ventilator (TOPO, Kent Scientific, Torrington, CT, USA), respectively. Using a flowmeter, flow rates of air, O_2, N_2, and CO_2 were adjusted to yield suitable blood gas measurements, determined from the femoral artery blood samples with a blood gas analyzer (Rapidlab 248, Bayer Healthcare, LLC East Walpole, MA, USA).

For pO_2 measurement, a solution of Oxyphor R2 in saline was administered through the femoral vein to yield a concentration of 40 μmol/L in the bloodstream.

Baseline Measurements

Absolute CBF and pO_2 were monitored in cortical vasculature under baseline conditions in 10 animals. During 200 seconds of baseline activity, pO_2 values were measured in select intravascular locations at 5-second intervals concurrent with volumetric OCT scans collected at 15-second intervals. Oxygen partial pressure was measured at 20 to 30 intravascular locations during each 5-second interval. At each location, phosphorescence was excited for 100 μs. The resultant phosphorescence emission decay profile was collected at 50 MHz sampling rate for 500 μs. Fifty decay profiles were averaged for each measurement ($\sim$30 ms per point measurement). The decay lifetime was calculated and converted to pO_2 (Sakadžić *et al*, 2009; Yaseen *et al*, 2009). The volumetric OCT scan consisted of $820 \times 160 \times 1024$ pixels over the $2 \times 2 \times 1.85$ mm^3 volume. The measured phase shifts were converted to velocity along the axial direction as described in Srinivasan *et al* (2010).

Somatosensory Stimulation

Planar OCT scans and intravascular pO_2 measurements were performed at selected points during somatosensory

stimulation in 10 rats. Each stimulus consisted of a train of current pulses ($\sim$2 mA amplitude, 300 μs duration) delivered to the forepaw at 3 Hz for 4 seconds with a 20-second interstimulus interval.

To determine the location, magnitude, and stability of the hemodynamic response, all animals were initially imaged with optical intrinsic signal imaging (OISI). Using a spectrally filtered Hg:Xe light source, the cranial window was illuminated with 570 nm light and imaged with a CCD camera (Photometrics Cascade 512F, Roper Scientific, Tucson, AZ, USA) at 25 frames/s during stimulation. The wavelength $\lambda = 570$ nm is an isosbestic point for oxyhemoglobin and deoxyhemoglobin. Consequently, an increase in blood volume, irrespective of oxygenation level, causes a local reduction of diffusely reflected light at the activated region.

To confirm that the region of maximal electrical activity coincides with the hemodynamically active area identified by OISI, surface potential measurements were also recorded in select animals using a silver ball electrode. The electrode was positioned at nine discrete locations along the cortical surface, and recordings were performed using identical stimulus conditions.

During the experiment, pO_2 values were measured at selected intravascular locations at either 1- or 0.5-second intervals, depending on the number of points measured per interval. To gain greater temporal resolution with the OCT measurements, a planar *xz* cross-section measuring roughly 2×1.85 mm^2 was repeatedly scanned at $\sim$250 ms intervals at 2730 axial scans per image.

Data Processing

Cerebral blood flow and pO_2 were calculated from the optical measurements using previously described processing methods (Srinivasan *et al*, 2009; Yaseen *et al*, 2009) implemented in either Matlab (Mathworks, Natick, MA, USA) or C. Unless stated otherwise, population data appear as mean $\pm$ sd.

Cerebral blood flow results were obtained from OCT Doppler measurements. The readout rate of the OCT system's camera limited the range of measurable velocities to $\pm$3.6 mm/s along the axial direction. Consequently, high axial velocity projections often resulted in aliasing of measurements from descending pial arterioles. The absolute CBF measurements presented here thus come only from ascending venules, obtained by integrating the measured Doppler phase shifts over the vessels' *xy* cross-sections (Srinivasan *et al*, 2010). For forepaw stimulation experiments, the *xz*-planar OCT scans measured vessels that were oriented orthogonally to the measured velocity component, thus providing relative flow measures in arterioles and venules (Srinivasan *et al*, 2009).

Intravascular pO_2 data were obtained from relating the calculated phosphorescence lifetime measurements to a calibration curve (Sakadžić *et al*, 2009). O_2 saturation (SO_2) was determined from the pO_2 measurements using the Hill equation ($n = 2.7$, P50 = 38 mm Hg) (Gray and Steadman, 1964).

For baseline experiments, pO_2 and flow measurements were used to calculate absolute O_2 extraction from individual ascending venules and their corresponding upstream microvasculature. Oxygen concentration was determined in diving arterioles and ascending venules as the sum of bound and dissolved oxygen, assuming that hematocrit, pH, and temperature did not vary during measurement (Ances *et al*, 2001). For each venule, the arteriovenous (AV) oxygen difference was calculated by subtracting the venular O_2 concentration from that of the animal's highest measured arteriolar O_2 concentration. O_2 extraction was determined as the product of each venules' absolute flow with the AV oxygen difference.

Temporal profiles obtained during somatosensory stimulation experiments were analyzed to evaluate dynamics of the CBF response and oxygenation. In addition to measuring the peak times, onset times for pO_2 and CBF were determined by finding t_{10}, the time required to increase from baseline value to 10% of the peak response, while rise times were computed as the difference between t_{90} and t_{10}. Return times were determined as the length of time after the peak required for the transient to return to 50% of the peak value. These profile characteristics were measured from CBF and pO_2 profiles of arterioles and veins and checked for statistical significance using paired *t*-tests.

Results

Baseline Conditions

Intravascular pO_2 and CBF measurements were simultaneously performed at 5- and 15-second intervals, respectively, in the superficial cortex under baseline conditions. Average arterial blood gas measurements across all animals were pO_2: 108.25 ± 11.02 mm Hg, pCO_2: 35.43 ± 3.29 mm Hg, pH: 7.39 ± 0.03.

Figures 2A–2C display angiograms of cortical microvasculature, collected by the confocal microscope. The images were created by temporally integrating the phosphorescence intensity at each pixel. Oxygen partial pressure measurements at selected intravascular locations are indicated by color-coded circles. Figures 2D–2F show corresponding OCT-based angiogram of the same cranial window preparations obtained by high-pass filtering the collected backscattered intensity signal (Srinivasan *et al*, 2010). Higher concentration of dissolved O_2 results in more phosphorescence quenching of Oxyphor R2. As a result, phosphorescence decays from points in arterioles have shorter lifetimes than in venules causing arterioles to appear darker in the confocal images. Conversely, the higher velocity of erythrocytes within arterioles generates greater Doppler shifts in the backscattered light, causing arterioles to appear brighter than veins in the OCT-based angiograms. As seen in Figures 2A–2C, pO_2 measurements vary considerably over extremely small distances.

Figures 2G and 2H display microvascular pO_2 and absolute flow measurements from all animals as a function of vessel diameter (d). Arteriolar pO_2 values were found to decrease substantially with vessel diameter, with statistically significantly lower pO_2 in arterioles $< 40\,\mu$m (Supplementary Figure 1).

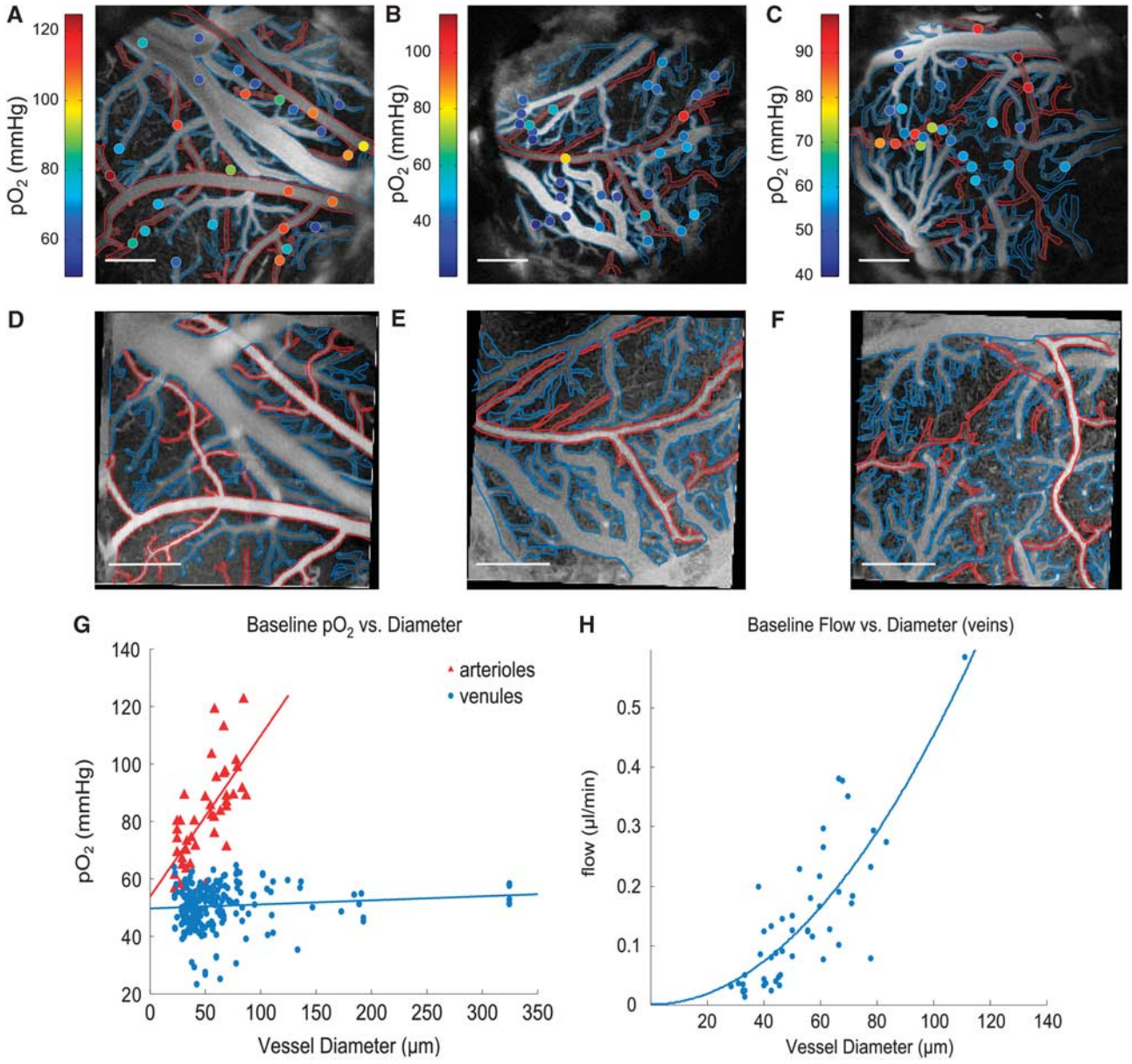

Figure 2 (**A**–**C**) Confocal-based angiograms of rat cerebral cortices, generated by phosphorescence intensity of exogenous Oxyphor R2 dye. Arterioles are outlined in red and venules are outlined in blue. Color-coded points indicate intravascular oxygen partial pressure (pO_2) measurements. (**D**–**F**) Corresponding optical coherence tomography (OCT)-based angiograms generated by scattering intensity. Scale bars: 500 μm. (**G**) pO_2 measurements in arteries and veins under baseline conditions, measured in 10 animals. Linear fits yielded $R^2 = 0.70$ and $R^2 = 0.10$ for arterioles and venules, respectively. (**H**) Absolute flow measurements in ascending venules under baseline homeostatic conditions, with associated quadratic fit ($R^2 = 0.65$).

Conversely, although pO_2 in venules showed pronounced variance, average values remained relatively consistent ($\sim$50 mm Hg) over all measured size ranges. Although pO_2 was fairly constant in the venules, flow increased from 0.05 ± 0.03 to 0.43 ± 0.22 μl/min as diameters increased from 20 to 100 μm. We characterized the spatial heterogeneity of pO_2 in arteries and venules, and CBF in venules, of different sizes by calculating the coefficient of variation (CV), computed as the ratio of the measurements' standard deviation to the mean (Pries *et al*, 1995; Shonat and Johnson, 1997). By normalizing the standard deviation by the mean, CV provides a more comparable, standardized indication of a measurement's dispersity than the standard deviation alone. As seen in Supplementary Figure 1, calculated CVs for pO_2 ranged from 0.120 to 0.190. For CBF measurements, CVs varied from 0.482 to 1.061.

Figure 3 illustrates the relationship between absolute oxygen extraction in units of μL/min and vessel diameter in ascending venules. Data points come from 10 separate animals in vessels whose

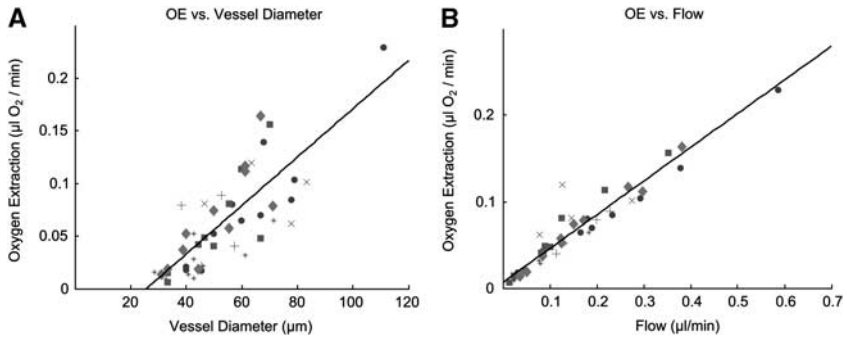

Figure 3 Absolute oxygen extraction (OE), calculated in microliters of O_2/min, in ascending venules of 10 animals under resting baseline conditions, with associated linear fits. Each symbol represents a specific animal. (**A**) OE versus vessel diameter ($R^2 = 0.80$) (**B**) OE versus absolute cerebral blood flow (CBF) ($R^2 = 0.96$).

diameters vary by a factor of 50. Each symbol corresponds to a specific animal. All data points fall upon a straight line in Figure 3B ($R^2 = 0.96$), the slope of which reinforces the homogeneity of pO_2 in ascending venules and implies a constant AV difference in O_2 concentration in the somatosensory cortex of all rats under baseline conditions.

Functional Activation

Oxygen partial pressure and rCBF measurements were simultaneously measured with high temporal resolution in the cortical microvessels of 10 animals during somatosensory stimulation. All animals were initially imaged with OISI to identify the location, magnitude, and stability of the hemodynamic response. In the three animals that were both imaged with OISI and whose stimulation-induced surface potentials were mapped with a silver ball electrode, we observed that the region with peak electrical activity coincided spatially with the centroid of the hemodynamically active area (Supplementary Figure 2). Immediately before stimulation experiments, arterial blood gas measurements were taken from the femoral artery of each animal, yielding the following average values: pO_2: 114.09 ± 11.41 mm Hg, pCO_2: 33.68 ± 3.58 mm Hg, pH: 7.41 ± 0.02.

Figures 4A and 4C depict representative, normalized profiles of pO_2 and CBF from individual arterioles and venules, respectively. The shaded region in each plot corresponds to the 4-second period during which an electrical stimulus was administered to the forepaw.

Figures 4B and 4D display peak changes of relative pO_2 (rpO_2) and rCBF, respectively, from arterioles and venules located <1 mm from the activation center. Peak changes in rpO_2 and rCBF correlated better with vessel diameter than with r, the distance from the centroid of hemodynamic activity (Supplementary Figures 3A and 3B), and the peak changes in rpO_2 and rCBF were more pronounced in venules than arterioles. Because of the large variance in the measurements, a strong relationship between peak rpO_2 or peak rCBF and vessel diameter is not apparent in venules; however, peak changes in rpO_2 and rCBF were consistently lower in larger arterioles than smaller ones. It must be noted, however, that the OCT system can currently only measure axial velocity projections within the range of ± 3.6 mm/s. Consequently, the system could not measure flow profiles in all arterioles within the activated region. Although the peak rCBF measurements from arterioles presented in Figure 4 all lie within the measurable range, the measurements depict only a subset of all the present arterioles.

The transient profiles for venules in Figure 4C reveal temporal lags between the pO_2 and CBF responses to functional activation. Table 1 presents the onset times, rise times, peak times, and return times for pO_2 and CBF transients in arterioles and veins, as averaged across all animals. Paired t-tests were performed for all observations in all animals. In arterioles, onset times, rise times, and peak times were not found to be significantly different for pO_2 and CBF responses. Conversely, in venules, all parameters were significantly different in pO_2 and CBF response ($P < 0.05$). Two-sample t-tests were used for comparison between arterioles and venules, which showed that pO_2 onset and return times were significantly different ($P < 0.05$) between arterioles and venules. Peak time differences for pO_2 responses in arterioles and venules were found to be nearly significant ($P = 0.0825$). Substantial differences in mean CBF onset times, rise times, and peak times were not found between arterioles and venules, and t-test analysis verified that the CBF response parameters were not significantly different.

To better illustrate baseline levels and stimulation-evoked peak changes in total oxygen content in pial microvessels, Figures 5A and 5B display baseline SO_2 and relative SO_2 changes in arterioles and venules categorized by diameter. Although the measurements displayed considerable variance, a multiple comparisons test revealed that the smallest arterioles (0 to 40 μm) have significantly lower ($\alpha = 0.05$) baseline O_2 content ($SO_2 = 82.61\%$) than larger arterioles ($SO_2 = 92.66\%$). As expected, O_2

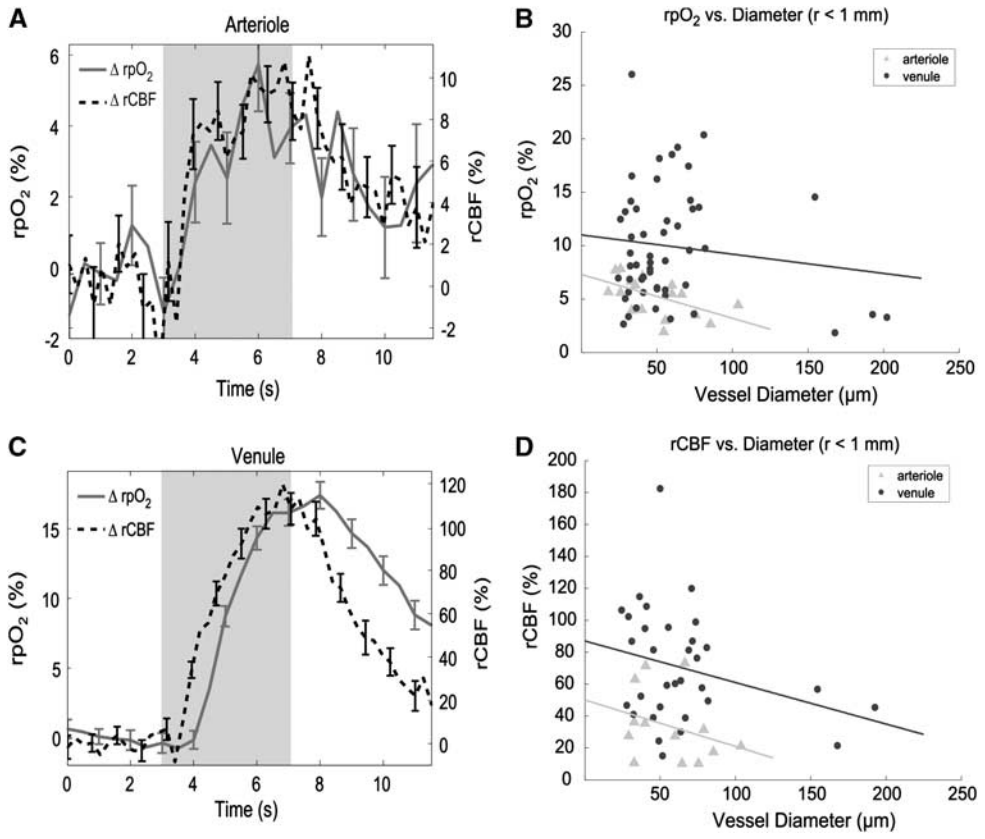

Figure 4 (**A**, **C**) Representative profiles of changes in relative oxygen partial pressure (rpO_2) and relative cerebral blood flow (rCBF) in (**A**) arterioles and (**C**) venules, in response to somatosensory stimulation. Error bars represent standard error. Shaded region corresponds to period of forepaw stimulation. (**B**) Peak changes in rpO_2 versus diameter, as measured in 10 animals. (**D**) Peak changes in rCBF versus diameter.

Table 1 Calculated parameters of transient pO_2 and CBF responses (mean ± standard error) from arterioles and veins during somatosensory stimulation, averaged across 10 animals

	t_{onset} *(seconds)*	*Rise time (seconds)*	t_{peak} *(seconds)*	t_{return} *(seconds)*
$pO_{2\,art}$	0.82 ± 0.16	1.72 ± 0.27	2.83 ± 0.24	6.38 ± 0.90
CBF_{art}	0.57 ± 0.04	1.30 ± 0.24	2.40 ± 0.40	3.43 ± 0.54
$pO_{2\,vein}$	1.22 ± 0.08	1.76 ± 0.14	3.27 ± 0.12	4.70 ± 0.30
CBF_{vein}	0.63 ± 0.05	1.40 ± 0.16	2.41 ± 0.18	3.95 ± 0.33

CBF, cerebral blood flow; pO_2, oxygen partial pressure.

content in all arterioles is still substantially higher than in venules. Smaller arterioles experienced larger absolute changes in SO_2 compared with larger arterioles. Mean baseline O_2 content in venules appeared to be quite similar ($SO_2 \sim 67.5\% \pm 10\%$), and all venules displayed comparable changes in peak SO_2 response ($\Delta SO_2 \sim 5\%$).

Discussion

Optical imaging is currently the only existing method to nondestructively measure cerebral activity *in vivo* with microscopic resolution. Stimulation-evoked changes in cerebral oxygenation and blood flow have been observed previously by combining techniques such as Clark microelectrodes with laser Doppler flowmetry (Masamoto *et al*, 2009; Vazquez *et al*, 2010), or phosphorescence quenching with either laser Doppler or with laser speckle imaging (Ances *et al*, 2001; Sakadžić *et al*, 2009). To our knowledge, however, the current study is the first to perform simultaneous, minimally invasive, and absolute measurements of both parameters in multiple individual microvascular locations with high spatial and temporal resolution.

Baseline Oxygen Partial Pressure

As seen in Figures 2A–2C, pO_2 measurements vary considerably over distances $< 50\,\mu m$. Measuring

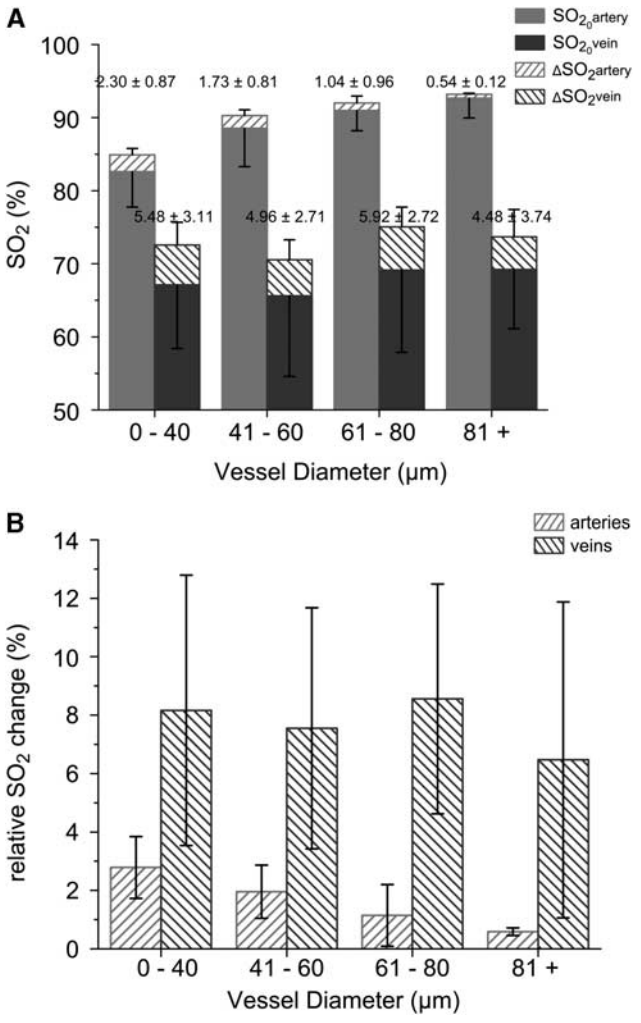

Figure 5 (**A**) Baseline O_2 saturation (SO_2) and stimulation-evoked changes in arterioles and venules, grouped by vessel diameter. Net SO_2 differences are provided above each bar. Upper portions of the error bars represent std of the peak change, while the lower portions represent std of the baseline SO_2 measurements. (**B**) Relative changes in SO_2 (normalized to baseline values) in arterioles and veins in response to somatosensory stimulation, grouped by vessel diameter.

these areas with conventional Clark electrodes, considered the gold standard technique for pO_2 measurement, could result in substantial spatial averaging. Under resting baseline conditions, arteriolar pO_2 values were found to decrease significantly, from 100.90 ± 18.67 mm Hg in pial arterioles with $d > 80\,\mu$m to 69.33 ± 9.11 mm Hg in pial arterioles with $d < 40\,\mu$m (Supplementary Figure 1). Our arteriolar pO_2 measurements are in general agreement with the baseline measurements of Vazquez *et al* (2008) and Vovenko (1999), who independently measured intravascular pO_2 in rat cerebral cortices using Clark-type microelectrodes. Our measurements support their conclusions from experiments in brain tissue, along with the conclusions of Duling and Berne (1970) from experiments in hamster cheek pouches and rat cremaster muscles, that tissue extracts nonnegligible amounts of O_2 from smaller arterioles under baseline conditions, challenging the conventional belief that O_2 diffusion from capillaries exclusively satisfies tissue's oxygen demand. Our results are also consistent with recent two-photon experiments, which revealed an absence of capillaries in cortical tissue surrounding diving arterioles (Kasischke *et al*, 2010), further corroborating the role of arterioles in tissue oxygenation. In that study, Kasischke *et al* performed two-photon imaging of endogenous nicotinamide adenine dinucleotide in mouse cortical tissue, and observed patches of diminished nicotinamide adenine dinucleotide fluorescence that colocalized with diving arterioles. These findings, together with the observations from our group showing pO_2 gradients in brain tissue near arterioles (Sakadžić *et al*, 2010), strongly support our belief that oxygen diffuses from the arterioles into the tissue. Together, the results challenge the suggestion that the observed relationship between arteriolar diameter and pO_2 is the result of O_2 consumption by smooth muscle cells lining the arterioles.

Although baseline pO_2 measurements of venules demonstrated considerable heterogeneity, average pO_2 was ~ 50 mm Hg in venules of all sizes. Although the measured venous pO_2 is considerably higher than reported pO_2 values in brain tissue, no relationships were found between vessel diameter and pO_2 in veins. Consequently, our data provide no evidence that cortical venules supply O_2 to tissue under baseline conditions. Interestingly, both Vazquez and Vovenko reported substantially lower average pO_2 values in venules (but with similar variance), ranging from 33.3 to 41.3 mm Hg in venules with sizes from 13 to 361.0 μm. This discrepancy in the venous measurements has important implications regarding estimates of total oxygen extraction and consumption by brain tissue. A potential, but unlikely, cause for this difference could be the different pO_2 measurement technique that we used. Although the phosphorescence-quenching method relies upon a different mechanism than Clark-style electrodes to measure pO_2, phosphorescence measurement is calibrated against pO_2 measured by electrodes over the physiological pO_2 range (Dunphy *et al*, 2002; Sakadžić *et al*, 2009). Baseline physiological conditions most likely do not account for the different venous pO_2 levels. Systemic blood gas measurements indicate that our baseline pO_2 conditions were higher than those used by Vovenko but lower than those of Vazquez. We believe the discrepancy is largely attributable to the different experimental parameters used in each study. During the measurements, animals in Vovenko's study spontaneously breathed room air under sodium pentobarbital anesthesia. Conversely, animals in Vazquez's study breathed a mixture of air ($\sim 90\%$) and O_2 ($\sim 10\%$) using a ventilator while under isoflurane anesthesia. Additionally, because their electrode measurements were performed on the superior surface of the veins, it is possible that the electrode

spatially averaged pO_2 from both the vessels and extravascular tissue. In our experiments, the Oxyphor R2 dye remained confined to the vasculature, and therefore our detected signal unequivocally reflects an intravascular measurement.

Baseline Cerebral Blood Flow

Numerous techniques exist to characterize CBF (Hyder, 2009). Among the most widely used techniques, MRI and positron emission tomography are noninvasive and provide CBF maps of the entire brain. Neither method, however, allows for absolute, quantitative CBF measurement in individual microvessels. Scanning-laser Doppler and laser speckle imaging can map CBF with higher spatial resolution, but do not provide absolute flow values and lack depth specificity. Two-photon microscopy and video microscopy can yield measures of red blood cell velocity and flux in vessels with high spatiotemporal resolution. Relating RBC flux measurements to absolute flow requires assumptions regarding intravascular pressure, flow profile, and vessel orientation. Autoradiography provides absolute measurements and is considered the gold standard for measuring CBF. However, autoradiographic measurement requires harvesting brain tissue postmortem and provides no information regarding temporal changes. Optical coherence tomography is the first reported technology that enables quantitative measurement of absolute flow in microvessels. Our results for absolute flow in ascending venules of the cortex are within the same range reported for cerebral venules in a previous OCT study by our group (Srinivasan *et al*, 2010), and they are in general agreement with flow estimates in rat mesenteric venules obtained from simulations using experimental RBC flux measurements performed with intravital microscopy (Pries *et al*, 1995). Additionally, simulation results from Pries *et al* show a similar increasing relationship between absolute flow and increasing vessel diameter. The higher flow values seen in venules with larger diameters support the intuitive notion that these venules drain larger tissue volumes compared with smaller venules. To evaluate the relationship between absolute CBF and venous diameter, we calculated polynomial fits of different orders with zero intercept for our observations ($y = ax^b$, $b = 1$, 2, 3, and 4). Interestingly, we found that a quadratic function best characterizes the relationship ($R^2 = 0.65$), as seen in Figure 2H. As CBF flow was determined by integrating the measured velocity component over the vessel area, the data suggest that average blood velocity is constant across the range of measured vessel diameters in veins under baseline conditions. Using the fitted quadratic relation, we computed the average velocity in venules to be ~ 0.96 mm/s.

Much of the variance in our pO_2 and CBF observations is attributable to varying physiological conditions across animals. However, we also found that pO_2 and CBF measurements displayed pronounced spatial heterogeneity within the same animal. Our calculated CVs for pO_2 were lower than CVs determined for intravascular pO_2 measurements in the rat spinotrapezius muscle (Shonat and Johnson, 1997). Coefficient of variations for our CBF measurements were comparable with CVs from estimated flow values in rat mesenteric venules (Pries *et al*, 1995).

Baseline O_2 Extraction

In light of the pronounced variance in both pO_2 and flow measurements, the constant relationship between total extracted oxygen and CBF in individual vessels across all animals is particularly noteworthy. Reports discussing CBF heterogeneity have suggested that variable efficiency of tissue oxygenation and capillary exchange of solutes account for the spatial and temporal heterogeneity of CBF (Duling and Damon, 1987). Our simultaneous measurements of pO_2 and flow under baseline conditions suggest a constant AV O_2 concentration difference in all ascending venules, implying that the efficiency of O_2 exchange from microvessels does not vary under baseline conditions. Assuming that larger venules drain from larger tissue volumes, our data suggest that CBF in a microvessel closely matches O_2 demand of the tissue that it supplies. This observation of constant O_2 extraction efficiency complements NIRS observation in healthy infants (Franceschini *et al*, 2007), which showed that SO_2 remains constant in developing brain tissue while CBV doubles in the first year of life. Both results imply that steady-state cerebral vascularization and flow is tightly coupled to oxygen demand (Pugh and Ratcliffe, 2003). In our case, the results suggest that large venules with higher flow drain larger tissue regions, presumably with more extensive capillary beds and oxygen demand compared with smaller venules.

Functional Activation

Forepaw stimulation induced increases in pO_2 and CBF in both arterioles and venules. In venules, peak rCBF and rpO_2 changes were considerably higher, as well as more dispersed, than arterioles. Interestingly, we measured rCBF changes in individual microvessels ranging from 10% to 80% in arterioles and from 15% to 180% in venules, and peak values decreased with increasing vessel diameter for both vessel types. As CBF changes are primarily manifested in the form of modulated arteriolar diameter (Hillman *et al*, 2007), and the venous compartment comprises more of the blood volume than arteriolar compartment, this observation challenges the assumption that rCBF changes would be more pronounced within arterioles. Numerous reasons may account for this counter-intuitive result. As baseline flow is higher in arterioles, a given change in absolute flow may

appear as a smaller relative change in arterioles compared with venules. Additionally, the localized stimulus-evoked increase in CBF may redistribute flow from baseline conditions, resulting in fewer, more proximal venules draining an activated arteriole than under baseline conditions. Lastly, because the range of measurable axial velocity projections by our system is currently limited to ±3.6 mm/s, the system is unable to measure baseline flows in all arterioles. The rCBF measurements from arterioles presented in Figure 4 lie within the measurable range and did not suffer from phase-wrapping or pulsatility artifacts; however, the measurements represent only a subset of all the arterioles in the functionally activated region. Therefore, it remains possible that if all arterioles could be measured, arterioles may experience similar or larger stimulus-evoked rCBF changes compared with venules. To resolve this issue, further investigation is necessary after modifying our OCT system to detect velocities over a larger range.

Figures 4B and 4D illustrate another interesting phenomenon in our results. Both peak rpO_2 and rCBF demonstrate considerable spatial heterogeneity during functional activation. Neither parameter was found to correlate well with distance from the activation center, determined by OISI (Supplementary Figures 3A and 3B). A modest correlation exists between the two measured quantities rpO_2 and rCBF (Supplementary Figure 3C). The correlation is consistent with the notion that vascular pO_2 changes are driven by flow-induced influx of more-highly oxygenated blood, and it suggests that rpO_2 heterogeneity follows rCBF heterogeneity. Both parameters also decrease with increasing vessel diameter. As mentioned previously, it is not well understood how CBF redistributes on a microvascular level in response to localized functional activity. The dispersity in our rCBF measurements may be a consequence of fewer, more proximal venules being recruited to drain a given activated arteriole compared with baseline conditions. Future investigations will explore the nature of this spatial heterogeneity under both baseline and functionally activated conditions.

By comparison, other forepaw stimulation studies in rats that used techniques such as MRI-based arterial spin labeling, OISI, laser speckle, and laser Doppler imaging have reported CBF increases of ~80% (Sicard and Duong, 2005; Silva *et al*, 1999), 15% (Dunn *et al*, 2005), 35% to 60% (Sakadžić *et al*, 2009), and 20% to 55% (Ances *et al*, 2001; Masamoto *et al*, 2009; Vazquez *et al*, 2010), respectively. Direct comparison between these investigations is confounded by the different experimental parameters, including anesthetic, baseline conditions, and stimulus parameters, used in each study. The techniques used in previous studies require substantial spatial averaging, and are likely biased toward larger vessels that provide greater signal. Compared with these techniques, OCT offers unique advantages by enabling the distinction between arterioles and venules, and also the ability to measure CBF changes in individual microvessels from the brain surface to subsurface depths beyond 1 mm.

As with our baseline measurements, our pO_2 observations show trends similar to those of Vazquez *et al* (2010), who performed pO_2 measurements with Clark microelectrodes during forepaw stimulation. Interestingly, our average changes in SO_2 were ~50% lower than their reported results. To an extent, their stimulus parameters, most notably longer stimulus duration, along with their lower baseline measurements may account for this discrepancy, particularly in the venous measurements. Also, their SO_2 results show larger variance, and therefore our average SO_2 changes fall within the range of their measurements. Similar to Vazquez's data, we observed that smaller arterioles experienced larger peak changes in both pO_2 and SO_2. This further supports the notion that O_2 extraction takes place from the arterioles upstream from the capillaries, both during baseline conditions and during functional activity (Vazquez *et al*, 2010; Vovenko, 1999). Our observations also showed significant delays between the onset, peak, and return time of the venous pO_2 response relative to the CBF response. As has been reported previously (Hillman *et al*, 2007), the delay in onset time mainly represents the time required for changes in arterial CBF to affect blood oxygenation levels downstream. The effect is a consequence of both the transit time through the capillary bed and changes in $CMRO_2$. Interestingly, the delay in return time between CBF and pO_2 was quite similar to that of onset time.

The Initial Dip

Several investigators have observed a small, transient increase in deoxyhemoglobin occurring at the onset of functional stimulation that precedes the larger CBF response. This deoxyhemoglobin increase, which manifests as an 'initial dip' on the fMRI BOLD signal and pO_2 profiles, is believed to represent a focal increase in cerebral oxygen metabolism that is dynamically uncoupled from CBF. The initial dip is not always observed and remains the subject of longstanding controversy (Buxton, 2001). It is also more frequently observed in optical imaging experiments than fMRI experiments. Tian *et al* (2010) recently reported that the initial dip is most prominent in superficial tissues, where the hemodynamic response is delayed compared with deeper, more metabolically active tissue in cortical layer IV. As optical measurements are inherently biased toward the tissue surface, this may explain why the dip is observed more frequently in optical imaging studies. Using the phosphorescence-quenching method, some investigators have reported observing the initial dip (Vanzetta and Grinvald, 1999) whereas others have not (Lindauer *et al*, 2001). Typically, in measured BOLD and pO_2 transients, the amplitude of

the initial dip is several times smaller than the subsequent increase brought on by the CBF response. The small amplitude, along with the temporal resolution and measurement variability in our experiments, make it difficult to determine conclusively whether the initial dip can be seen in our pO_2 measurements. A small subset of pO_2 profiles were recorded where the initial dip may be evident. Select profiles are presented in Supplementary Figure 4. To further explore the nature of the initial dip, future studies will focus on obtaining measurements with higher temporal resolution and less variability.

Arteriolar Contribution to the Blood Oxygen Level Dependent Response

Our results also have implications regarding the role of arterioles in the BOLD response measured with fMRI. In general, the detected BOLD response is attributed primarily to increased venous oxygenation and blood volume. This is predicated largely on the assumptions that blood in the supplying arteries is fully saturated with oxygen and that veins compose a higher fraction of CBV than capillaries or arteries ($\sim$70% in veins versus $\sim$25% in arteries) (Kim *et al*, 2007; Lee *et al*, 2001). Our results demonstrate that blood is not completely oxygen saturated in arterioles under baseline conditions or during functional activity, and therefore deoxyhemoglobin concentration in arterioles is greater than zero and decreases during stimulation. This result, coupled with reported observations demonstrating larger stimulus-evoked increases in CBV within arterioles compared with veins (Hillman *et al*, 2007; Kim *et al*, 2007), strongly supports the suggestion that the contribution of arterioles to the BOLD response may be underestimated (Hillman *et al*, 2007). Our analysis of temporal profiles suggest that arteriolar pO_2 changes concomitantly with CBF, whereas the pO_2 changes in venules lagged behind CBF changes by $\sim$0.6 seconds. The relationships between the pO_2 and CBF transients support the possibility that arterioles may contribute to the onset and early portion of stimulus-induced BOLD response, while changes in CBV, CBF, and oxygenation in venules account for the later portion.

Our custom-built multimodal system allows for simultaneous, high-resolution measurement of cerebral oxygenation and blood flow in multiple intravascular locations. In the future, the system could be useful for investigating the nature of the stimulus-evoked decrease in blood oxygenation reported in several fMRI and optical imaging studies (Shmuel *et al*, 2002; Devor *et al*, 2007). Specifically, simultaneous CBF and pO_2 measurements could help determine whether the negative BOLD response is the result of the 'vascular steal' phenomenon. Currently, the system is limited by the penetration depth of confocal microscopy and the OCT component's range of measurable velocities. By extending the system to exploit novel two-photon sensitive dendritic phosphor PtP-C343 (Finikova *et al*, 2008), we recently demonstrated minimally invasive intravascular and extravascular pO_2 measurements at subsurface depths of 240 μm (Sakadžić *et al*, 2010). These results encourage ongoing modifications of our system to enable simultaneous intravascular and extravascular pO_2 measurements with two-photon microscopy together with OCT measurements of CBF in microvessels over a broader range of velocities. Such results would allow for calculation of $CMRO_2$ with unprecedented spatial and temporal resolution.

Conclusions

We have constructed and used a multimodal microscope system capable of simultaneous CBF and pO_2 measurements in cortical vasculature with high spatial and temporal resolution. Under both baseline conditions and during functional activity, CBF and pO_2 vary substantially across distances that currently cannot be resolved using conventional brain imaging techniques, illustrating the need for measurement techniques at multiple locations with high spatial and temporal resolution. Despite the heterogeneity in pO_2 and CBF, the nearly constant AV difference in O_2 concentration suggests that CBF is matched to O_2 demand in brain tissue at the level of individual draining vessels. Arteriolar pO_2 decreased significantly with decreasing diameter, and larger rises in cerebral pO_2 were observed in smaller arterioles during functional stimulation. Both of these observations support the belief that arterioles supply O_2 to brain tissue and contribute to the BOLD response.

Our system demonstrates the potential to yield high-resolution quantification of $CMRO_2$. It could also lead to better interpretation of the BOLD response and a more comprehensive understanding of metabolic dynamics under various neuropathologies.

Acknowledgements

The authors gratefully acknowledge Dr Sergei Vinogradov and Svetlana Ruvinskaya for invaluable help with pO_2 experiments and scrupulous manuscript editing.

Disclosure/conflict of interest

The authors declare no conflict of interest.

References

Ances BM, Wilson DF, Greenberg JH, Detre JA (2001) Dynamic changes in cerebral blood flow, O_2 tension, and calculated cerebral metabolic rate of O_2 during functional activation using oxygen phosphorescence quenching. *J Cereb Blood Flow Metab* 21:511–6

Atwell D, Iadecola C (2002) The neural basis of functional brain imaging signals. *Trends Neurosci* 25:621–5

Bartlett K, Saka M, Jones M (2008) Polarographic electrode measures of cerebral tissue oxygenation: implications for functional brain imaging. *Sensors* 8:7649–70

Boas DA, Strangman G, Culver JP, Hoge RD, Jasdzewski G, Poldrack RA, Rosen BR, Mandeville JB (2003) Can the cerebral metabolic rate of oxygen be estimated with near-infrared spectroscopy? *Phys Med Biol* 48:2405–18

Buxton RB (2001) The elusive initial dip. *Neuroimage* 13:953–8

Buxton RB (2010) Interpreting oxygenation-based neuroimaging signals: the importance and the challenge of understanding brain oxygen metabolism. *Front Neuroenergetics* 2:8

Devor A, Tian P, Nishimura N, Teng IC, Hillman EMC, Narayanan SN, Ulbert I, Boas DA, Kleinfeld D, Dale AM (2007) Suppressed neuronal activity and concurrent arteriolar vasoconstriction may explain negative blood oxygenation level-dependent signal. *J Neurosci* 27: 4452–9

Duling BR, Berne RM (1970) Longitudinal gradients in periarteriolar oxygen tension: a possible mechanism for the participation of oxygen in local regulation of blood flow. *Cir Res* 27:669–78

Duling BR, Damon DH (1987) An examination of the measurement of flow heterogeneity in striated muscle. *Cir Res* 60:1–13

Dunn AK, Devor A, Dale AM, Boas DA (2005) Spatial extent of oxygen metabolism and hemodynamic changes during functional activation of the rat somatosensory cortex. *Neuroimage* 27:279–90

Dunphy I, Vinogradov SA, Wilson DF (2002) Oxyphor R2 and G2: phosphors for measuring oxygen by oxygen-dependent quenching of phosphorescence. *Anal Biochem* 310:191–8

Finikova OS, Lebedev AY, Aprelev A, Troxler T, Gao F, Garnacho C, Muro S, Hochstrasser RM, Vinogradov SA (2008) Oxygen microscopy by two-photon-excited phosphorescence. *ChemPhysChem* 9:1673–9

Franceschini MA, Thaker S, Themelis G, Krishnamoorthy KK, Bortfeld H, Diamond SG, Boas DA, Arvin K, Grant EP (2007) Assessment of infant brain development with frequency-domain near-infrared spectroscopy. *Pediatr Res* 61:546–51

Gray LH, Steadman JM (1964) Determination of the oxyhaemoglobin dissociation curves for mouse and rat blood. *J Physiol (Cambridge)* 175:161–71

Hillman EMC, Devor A, Bouchard MB, Dunn AK, Krauss GW, Skoch J, Backsai BJ, Dale AM, Boas DA (2007) Depth-resolved optical imaging and microscopy of vascular compartment dynamics during somatosensory stimulation. *Neuroimage* 35:89–104

Hyder F (2009) Dynamic imaging of brain function. In: *Dynamic Brain Imaging: Multi-Modal Methods and In Vivo Applications* (Hyder F, ed), Totowa, NJ: Humana Press, pp 3–21

Kasischke KA, Lambert EM, Panepento B, Sun A, Gelbard HA, Burgess RW, Foster TH, Nedergaard M (2010) Two-photon NADH imaging exposes boundaries of oxygen diffusion in cortical vascular supply regions. *J Cereb Blood Flow Metab* In Press

Kim T, Hendrich KS, Masamoto K, Kim S-G (2007) Arterial versus total blood volume changes during neural activity-induced cerebral blood flow change: implication for BOLD fMRI. *J Cereb Blood Flow Metab* 27: 1235–47

Kwong KK, Belliveau JW, Chesler DA, Goldberg IE, Weisskoff RM, Poncelet BP, Kennedy DN, Hoppel BE, Cohen MS, Turner R, Cheng H-M, Brady TJ, Rosen BR (1992) Dynamic magnetic resonance imaging of human brain activity during primary sensory stimulation. *Proc Natl Acad Sci USA* 89:5675–9

Lee S-P, Duong TQ, Yang G, Iadecola C, Kim S-G (2001) Relative changes of cerebral arterial and venous blood volumes during increased cerebral blood flow: implications for BOLD fMRI. *Magn Reson Med* 45:791–800

Leitgeb R, Hitzenberger CK, Fercher AF (2003) Performance of Fourier domain versus time domain optical coherence tomography. *Opt Express* 11:889–94

Leontiev O, Dubowitz DJ, Buxton RB (2007) CBF/$CMRO_2$ coupling measured with calibrated BOLD fMRI: sources of bias. *Neuroimage* 36:1110–22

Lindauer U, Royl G, Leithner C, Kühl M, Gold L, Gethmann J, Kohl-Bareis M, Villringer A, Dirnagl U (2001) No evidence for early decrease in blood oxygenation in rat whisker cortex in response to functional activation. *Neuroimage* 13:988–1001

Masamoto K, Vazquez A, Wang P, Kim S-G (2009) Brain tissue oxygen consumption and supply induced by neural activation: determined under suppressed hemodynamic response conditions in the anesthetized rat cerebral cortex. In: *Oxygen Transport to Tissue XXX* (Liss P, Hansell P, Bruley DF *et al*, eds), New York, NY: Springer Science+Business Media, LLC, pp 287–92

Pries AR, Secomb TW, Gaehtgens P (1995) Structure and hemodynamics of microvascular networks: heterogeneity and correlations. *Am J Physiol* 269:H1713–22

Pugh CW, Ratcliffe PJ (2003) Regulation of angiogenesis by hypoxia: role of the HIF system. *Nat Med* 9:677–85

Riera JJ, Schousboe A, Waagepetersen HS, Howarth C, Hyder F (2008) The micro-architecture of the cerebral cortex: functional neuroimaging models and metabolism. *Neuroimage* 40:1436–59

Rumsey WL, Vanderkooi JM, Wilson DF (1988) Imaging of phosphorescence: a novel method for measuring oxygen distribution in perfused tissue. *Science* 241:1649–51

Sakadžić S, Roussakis E, Yaseen MA, Mandeville ET, Devor A, Lo EH, Vinogradov SA, Boas DA (2010) Imaging of oxygen partial pressure in cerebral vasculature and tissue using a two-photon-enhanced phosphorescent nanoprobe. *Nat Methods* 7:755–9

Sakadžić S, Yuan S, Dilekoz E, Ruvinskaya S, Vinogradov SA, Ayata C, Boas DA (2009) Simultaneous imaging of cerebral partial pressure of oxygen and blood flow during functional activation and cortical spreading depression. *Appl Opt* 48:D169–77

Shmuel A, Yacoub E, Pfeuffer J, Van de Moortele P-F, Adriany G, Hu X, Ugurbil K (2002) Sustained negative BOLD, blood flow and oxygen consumption and its coupling to the positive response in the human brain. *Neuron* 36:1195–210

Shonat RD, Johnson PC (1997) Oxygen tension gradients and heterogeneity in venous microcirculation: a phosphorescence quenching study. *Am J Physiol* 272:H2233–40

Sicard KM, Duong TQ (2005) Effects of hypoxia, hyperoxia, and hypercapnia on baseline and stimulus-evoked BOLD, CBF, and $CMRO_2$ in spontaneously breathing animals. *Neuroimage* 25:850–8

Silva AC, Lee S-P, Yang G, Iadecola C, Kim S-G (1999) Simultaneous blood oxygenation level-dependent and cerebral blood flow functional magnetic resonance imaging during forepaw stimulation in the rat. *J Cereb Blood Flow Metab* 19:871–9

Sokoloff L (1992) The brain as a chemical machine. In: *Progress in Brain Research* (Yu ACH, Hertz L, Norenberg MD *et al*, eds), Amsterdam: Elsevier Science, pp 19–33

Sokoloff L (2008) The physiological and biochemical bases of functional brain imaging. *Cogn Neurodyn* 2:1–5

Srinivasan VJ, Sakadžić S, Gorczynska I, Ruvinskaya S, Wu W, Fujimoto JG, Boas DA (2009) Depth-resolved microscopy of cortical hemodynamics with optical coherence tomography. *Opt Lett* 34:3086–8

Srinivasan VJ, Sakadžić S, Gorczynska I, Ruvinskaya S, Wu W, Fujimoto JG, Boas DA (2010) Quantitative cerebral blood flow with optical coherence tomography. *Opt Express* 18:2477–94

Tian P, Teng IC, May LD, Kurz R, Lu K, Scadeng M, Hillman EMC, De Crespigny AJ, D'Arceuil HE, Mandeville JB, Marota JJA, Rosen BR, Liu TT, Boas DA, Buxton RB, Dale AM, Devor A (2010) Cortical depth-specific microvascular dilation underlies laminar differences in blood oxygenation level-dependent functional MRI signal. *Proc Natl Acad Sci USA* 107:15246–51

Vafaee MS, Gjedde A (2004) Spatially dissociated flow-metabolism coupling in brain activation. *Neuroimage* 21:507–15

Vanzetta I, Grinvald A (1999) Increased cortical oxidative metabolism due to sensory stimulation: implications for functional brain imaging. *Science* 286:1555–8

Vazquez AL, Fukuda M, Tasker ML, Masamoto K, Kim S-G (2010) Changes in cerebral arterial, tissue, and venous oxygenation with evoked neural stimulation: implications for hemoglobin-based functional neuroimaging. *J Cereb Blood Flow Metab* 30:428–39

Vazquez AL, Masamoto K, Kim S-G (2008) Dynamics of oxygen delivery and consumption during evoked neural stimulation using a compartment model and CBF and tissue pO_2 measurements. *Neuroimage* 42:49–59

Vinogradov SA, Lo L-W, Wilson DF (1999) Dendritic polyglutamic porphyrins: probing porphyrin protection by oxygen-dependent quenching of phosphorescence. *Chem Eur J* 5:1338–47

Vovenko EP (1999) Distribution of oxygen tension on the surface of arterioles, capillaries, and venules of brain cortex and in tissue in normoxia: an experimental study on rats. *Pfluegers Archiv Eur J Physiol* 437:617–23

Yaseen MA, Srinivasan VJ, Sakadžić S, Wu W, Ruvinskaya S, Vinogradov SA, Boas DA (2009) Optical monitoring of oxygen tension in cortical microvessels with confocal microscopy. *Opt Express* 17:22341–50

Supplementary Information accompanies the paper on the Journal of Cerebral Blood Flow & Metabolism website (http://www.nature.com/jcbfm)